Constructing the model

Note: All references cited in this Supplement are listed at the end of the Supplement and all citation numbers refer to that list, not the list of references in the main text.

The model of ion permeation through the open RyR channel is a refinement of the model described in Ref. (1) that includes new mutation data (2) that was not available when the first model was created. Specifically, two charge-neutralizing mutations of aspartates in the cytosolic (*cis*) vestibule of the pore (D4938N and D4945N) were shown to affect RyR conductance and selectivity: the conductances in 250 mM symmetric KCl were 65% and 92% of WT for D4938N and D4945N, respectively, and permeability ratios P_{Ca}/P_K were reduced from 7.0 to 3.3 and 6.5. Charge-neutralizing mutations (D or E to N or Q) of other charged amino acids in the cytosolic vestibule did not affect either K^+ conductance or Ca^{2+} vs. K^+ selectivity (2).

Previous experiments (3,4) showed that neutralizing the charge on two negatively-charged amino acids (Asp-4899 and Glu-4900) significantly reduced both conductance and selectivity: the conductances in 250 mM symmetric KCl were 20% and 56% of WT for D4899N and E4900Q, respectively, and permeability ratios P_{Ca}/P_K were reduced from 7.0 to 3.4 and 3.2. Except for the mutation E4902Q, charge-neutralizing mutations of other charged amino acids in the lumenal vestibule did not affect either K^+ conductance or Ca^{2+} vs. K^+ selectivity. While the conductance of E4902Q was found to be similar to WT, a small but statistically significant change from WT in Ca^{2+} selectivity was found (4) so E4902 was also included in this model.

Only Asp-4899 and Glu-4900 were explicitly included in the first model of RyR (1), although a region of negative charge in the cytosolic vestibule was required to reproduce the data. In hindsight, these were the then-unknown Asp-4938 and Asp-4945. In the model described here, all of the charged amino acids found in mutation experiments to affect RyR conductance and selectivity (while still producing functional and caffeine- and ryanodine-sensitive channels) were included: Asp-4899 in the selectivity filter, Asp-4938 and Asp-4945 in the cytosolic vestibule, and Glu-4900 and Glu-4902 in the lumenal vestibule (Fig. 1).

Since no high-resolution structures of the RyR are available, it was necessary to reverse-engineer the location of these amino acids. Several low-resolution electron microscopy structures of the entire RyR protein in the closed state that were published after the initial model were used to guide this revision of the model pore (5,6). Construction of the model pore was done in a way similar to that described in Ref. (1), but the basic method is outlined here. Because of the homology between RyR and the potassium channel (6), the pore was given a narrow selectivity filter with a wider cytosolic vestibule. The selectivity filter radius was chosen to be the same as in the previous model (4 Å) and 15 Å in length. Homology models derived from low-resolution structures of the RyR pore indicate that the selectivity filter includes residues 4894 to 4899 (GGGIGD) (5). The model selectivity filter is long enough to include these amino acids, but only Asp-4899 is explicitly modeled (Fig. 1). The cytosolic vestibule radius was chosen to be 7 Å, consistent with low-resolution RyR structures (M. Samsó, Harvard Medical School, personal communication, 2007), although the model cannot distinguish between different vestibule radii as it can between different selectivity filter radii (Fig. 15 of Ref. (1)).

As in the previous model, Glu-4900 was placed at the selectivity filter/lumenal vestibule junction. Glu-4902 was placed on the lumenal face of the channel. These are in accordance with other modeling of the RyR pore based on KcsA homology and mutation experiments (Fig. 2 of Ref. (4)). Asp-4938 was placed in the cytosolic vestibule in accordance with homology modeling from low-resolution RyR structures and 15 Å away from Asp-4899 (5). Asp-4945 was

placed 10 Å away from Asp-4938 toward the cytosolic end of the pore (5,6) because, as part of the same α-helix, they are approximately two helix turns apart. Because the structure of the RyR pore in the open state has not yet been determined at a resolution sufficient to distinguish the conformation of the inner helices, the increase in pore radius near Asp-4945 was arbitrarily chosen to be 45°. The model is not sensitive enough to distinguish between different helix tilt angles.

Each of the aspartates and glutamates were assumed to be fully-charged and facing into the permeation pathway with the terminal carboxyl (COO^-) group on a flexible tether than can span a hemisphere of radius 5 Å for aspartates and 7 Å for glutamates (Fig. 1). In the one-dimensional Poisson-Nernst-Planck/Density Functional Theory (PNP/DFT) model (1,7), residues Asp-4938, Asp-4899, and Glu-4900 were modeled as two, independent, half-charged oxygen ions (2.8 Å diameter) confined to a region of the long axis of the pore spanned by each residue's hemisphere (1,8-11). For example, the centers of the oxygens for Asp-4899 were confined to 15 Å $< x <$ 25 Å in Fig. 1. The other residues in the model (Asp-4945 and Glu-4902) were modeled as regions of uniform fixed charge (i.e., just a background charge and not as ions that take up space) because the pore radius where they were located was too wide for the residues to exert excluded-volume effects on the permeating ions; their presence was only felt electrostatically by the permeating ions.

Many important structural inferences were made from the first model (1) that have not changed in this model (e.g., selectivity filter radius of 4 Å and the location of Glu-4900 at the selectivity filter/lumenal vestibule interface and that its range of tethered movement overlapped with that of Asp-4899). Other structural parameters were constrained by known structural information (e.g., distance of Asp-4938 from Asp-4899 or distance of Asp-4945 from Asp-4938) or were chosen to have a reasonable value (e.g., range of tethered movement of side chains, location of Glu-4902, or pore radius in the cytosolic vestibule). The results were insensitive to the exact choice of these latter values. Given the constraints of the previous model and known structural information and the insensitivity of the other parameters, there were no adjustable parameters with respect to the structure in this model.

There were, however, some parameters for the ions that had to be determined from the experimental data: the diffusion coefficients of the permeating ions and water are inputs to the PNP/DFT model. Because water does not contribute to the current and Cl^- does not permeate the channel, these were given diffusion coefficients of 1% of bulk within the pore. Previously it was shown that the results of the model did not change even when bulk diffusion coefficients were used (1). For the cations, three different diffusion coefficients were used within the pore, one in each of the following regions: in the cytosolic vestibule where Asp-4938 was confined (0 Å $< x <$ 10 Å), in the selectivity filter (10 Å $< x <$ 25 Å), and in the lumenal vestibule (25 Å $< x <$ 32 Å). In all other regions, bulk (infinite dilution) diffusion coefficients were used. The resulting piecewise constant profile was smoothed as described (1).

For K^+ the three diffusion coefficients were determined by reproducing the experimental current in symmetric 250 mM KCl in native RyR (80 pA at +100 mV) and in the mutants E4900Q (10 pA at +20 mV) and D4839N (52 pA at +100 mV). The diffusion K^+ coefficients (from cytosolic to lumenal) were 122.1×10^{-11}, 6.91×10^{-11}, and 40.3×10^{-11} m^2/s. For all non-K^+ cations (Li^+, Na^+, Rb^+, Cs^+, Mg^{2+}, and Ca^{2+}) only one diffusion coefficient was left undetermined by assuming that the ratio of bulk to cytosolic vestibule diffusion coefficients for K^+ was the same as for all other cations and by assuming that the ratio of selectivity filter to lumenal vestibule diffusion coefficients for K^+ was the same for all other cations. The one open diffusion

coefficient in the selectivity filter was determined for the monovalent cations by reproducing the current at +100 mV in 250 mM symmetric conditions: Li^+ (21.2 pA), Na^+ (48.1 pA), Rb^+ (71.5 pA), and Cs^+ (51.9 pA). For the divalent cations, the selectivity filter diffusion coefficient was determined by reproducing the current at –100 mV in 250 mM symmetric KCl and 10 mM lumenal divalent-chloride: Mg^{2+} (–31 pA) and Ca^{2+} (–33 pA). The selectivity filter diffusion coefficients were found to be: 1.29×10^{-11} for Li^+, 3.65×10^{-11} for Na^+, 6.91×10^{-11} for K^+, 5.92×10^{-11} for Rb^+, 4.18×10^{-11} for Cs^+, 0.42×10^{-11} for Mg^{2+}, and 0.41×10^{-11} m^2/s for Ca^{2+}.

While no molecular dynamics simulations to determine diffusion coefficients inside a highly-charged calcium channel have been performed, these values for the selectivity filter diffusion coefficients are consistent with those used in other models of RyR (12-14) and consistent with diffusion coefficients used in models of other highly-charged ion channels (7,15-18) and of other channels (19-23). Diffusion coefficients in highly-charged pores like RyR have never been simulated, so it is unclear how large they are. It is known, however, that concentrating electrolytes can significantly reduce their diffusion coefficients (24,25).

With some simplifying assumptions one can also do a back-of-the-envelope calculation to determine the order of magnitude of the selectivity filter diffusion coefficients. Assuming that the one-dimensional Nernst-Planck equation applies and that the baths are identical, one can integrate Eq. **Error! Reference source not found.** to give

$$g_i = \frac{z_i^2 e^2}{kT}\left[\int \left(D_i A \rho_i\right)^{-1} dx\right]^{-1} \tag{S1}$$

where the conductance $g_i = z_i e J_i / V$. If the flux is limited in the selectivity filter where the diffusion coefficient and area are constant and if the cation density is also assumed constant, then

$$g_i = \frac{z_i^2 e^2}{kT}\frac{D_i A \rho_i}{L} \tag{S2}$$

where L is the length of the selectivity filter. If there is only one cation species as the charge carrier, then charge neutrality gives $\rho_i \approx Q / z_i AL$ where Q is the number of negative protein charges in the selectivity filter. Then

$$g_i = \frac{z_i e^2}{kT}\frac{D_i Q}{L^2}. \tag{S3}$$

(Note that this estimate is independent of how the chemical potential is calculated.) In RyR, K^+ has a conductance of 800 pS (26). This corresponds to $D_K = 7.3\times10^{-11}$ m^2/s for a 15 Å-long selectivity filter with four negative protein charges—very close to the 6.91×10^{-11} m^2/s used in the model. Similarly, for Ca^{2+} with a conductance of 120 pS (Fig. S9A–C, open triangles), $D_{Ca} = 0.54\times10^{-11}$ m^2/s which is close to the 0.41×10^{-11} m^2/s used in the model. It is usually estimated that diffusion coefficients in narrow pores are reduced by at most a factor 10 from bulk. In this case, because the ion density ρ_i is very large (13 M for the Asp-4899 region (1)), if the diffusion coefficient is reduced by only a factor 10 from bulk, then the K^+ conductance would be about 2200 pS—2.75 times too large.

After determining the three diffusion coefficients for K^+ and one diffusion coefficient for Li^+, Na^+, Rb^+, Cs^+, Mg^{2+}, and Ca^{2+} using exactly 9 experimental data points out of more than a thousand, the model reproduces all the permeation and selectivity data of RyR2 (the cardiac isoform of RyR) in over 100 different ionic solutions—some yet to be published—*without readjusting any parameters*. The comparison of the revised model and experimental data for two mole fraction curves and 55 current/voltage curves in pure monovalent-chloride, biionic, and monovalent/divalent mixtures in native and mutant RyR of Ref. (1) are shown here and in the

main text. Comparisons of model results and previously unpublished experiment data will be published later.

The additional structural and mutation data have substantially improved the results of the model. The new model also reproduces the conductances of mutations not in the previous model without any adjustable parameters; in 250 mM symmetric KCl, the model conductance is 718 pS for D4945N (experimental 737±11 pS (2)) and 792 pS for E4902Q (experimental 782±4 pS (4)).

Details of the modeling not described here are discussed in Ref. (1).

Figs. S1-S9 show the results of the model compared to experiments in 66 ionic solutions in both native and three mutants (D4899N, E4900Q, and D4938N). These experimental data have been published previously (1,2,4) and many were compared to the previous model (1). Figs. S1–S9 compare this same data to the new model because there were important improvements in many cases (see figure captions). While not all comparisons showed improvement, the entire data set is included for completeness.

Testing consistency of the model

In the model, ions are charged, hard spheres and water is a fluid of hard spheres, all moving through RyR via one-dimensional drift-diffusion (PNP). Selectivity occurs when the ions interact with the five amino acids described above. Figs. S1–S9 in the Appendix show how the results of this model compare to experiments; Figs. 1–12 show the results of the analysis of the main text. Given how well the model reproduces the experimental data and that it can predict other data, this minimalist model seems to capture the essential physics of ion permeation and selectivity in RyR. On the other hand, the model does not include several energies usually included in other models of ion permeation and selectivity. At the same time, the diffusion coefficients seem unusually small. It is important to check the consistency of the model with respect to these issues:

Water as hard spheres. This model of water can reproduce relatively accurate values of the bath activity coefficients (Appendix of 1) which is important to reproduce the reversal potentials of the current/voltage curves. It does not, however, have any attractive ion/water interactions. The success of the model in reproducing the experimental data then suggests that there is only a small net energy step from ion dehydration as the ion enters the channel and resolvation by the COO^- of the protein charges. This is consistent with the experimental data of Mg^{2+} and Ca^{2+} and their mixtures with K^+. Fig. S9A and D shows that as more and more divalent is added to the lumenal side, the conductances at negative voltages are very similar; they differ by at most 10% at 50 mM divalent. If dehydration/resolvation were very important, it would show in this experiment since Mg^{2+} and Ca^{2+} have a 130 kT difference in dehydration energy (27). For example, at 5 mM divalent (Fig. S9A and D, solid squares), the current/voltage curves of Mg^{2+} and Ca^{2+} mixtures with K^+ are virtually identical, indicating the Mg^{2+} does not have difficulty entering the channel compared to Ca^{2+}; they both compete equally well with K^+. Gouaux and MacKinnon have suggested that a highly-charged selectivity filter can resolvate the ions to overcome any dehydration penalty (28); the net energy of an ion entering the pore is the sum of two terms that virtually cancel. The prediction of the model that the ion dehydration/resolvation step is small must be tested and will be explored in future work. If true, it is likely that this true only for RyR and a small number of other channels.

The dielectric coefficient of the entire system is 78.4. It is reasonable to assume that the dielectric coefficient of both the channel lumen and the channel protein is less (and possibly significantly less) than 78.4. Via Born energies, a low dielectric in the lumen is equivalent to an

ion dehydration/resolvation penalty which, empirically, seems to be small; the dielectric coefficient within the pore seems to be high in this 8 Å-wide channel. An alternate explanation is that the screening component of the chemical potential includes a Born-like energy. In the mean spherical approximation of ions in bulk solutions (Eq. (16) of 8), the screening term is (to first-order) proportional to z_i^2 and inversely proportional to an effective ion radius—just like the Born energy. How much this compensation may be is difficult to estimate before more detailed studies on ion dehydration/resolvation are done.

On the other hand, a high protein dielectric coefficient is consistent with RyR having millimolar Ca^{2+} affinity (10,11) since a low-dielectric protein significantly increases Ca^{2+} affinity. This counter-intuitive result is due to the charges that ions induce on the protein/lumen dielectric interface. Boda et al. (10,11) have shown that in a highly-charged selectivity filter like in RyR, the negative protein charges induce negative charges on this interface that attract more cations. In these simulations, the number of ions inside the pore changed by a factor 2–3 at millimolar [Ca^{2+}] when the protein dielectric constant had a value between 2 and 10. However, these low protein dielectric constants increased Ca^{2+} affinity by 5- to 10-fold beyond RyR's millimolar affinity (10,11). Therefore, it is likely that the RyR protein dielectric constant is not significantly smaller than the 78.4 used in the RyR model (probably 40 or above). The Boltzmann factor of an error due to the protein dielectric constant will thus be small (<1 kT for a 50% error in pore concentrations). As with any net change in Boltzmann factor, some terms in the chemical potential (e.g., excluded-volume) will become more positive and other terms (e.g., screening) will become more negative. Work is currently underway to incorporate different dielectric coefficients into the DFT.

The diffusion coefficients are very small. In the Appendix, a back-of-the-envelope calculation is presented that shows that a one-dimensional PNP approach where diffusion is limited in a highly-charged selectivity filter necessarily requires the very small diffusion coefficients used in the model. The calculation does not, however, indicate whether those diffusion coefficients are physically real. The diffusion coefficients of ions inside a highly-charged channel are currently not known. Only diffusion coefficients in weakly-charged pores have been computed by molecular dynamics (22,25,29). Work is currently under way to compute diffusion coefficients in a narrow DDDD locus.

The calculation in the Appendix also does not indicate whether the assumptions of the model are true; for example, in the model of Corry et al. (30) flux is not only limited in the selectivity filter, but also in one of the vestibules with a dielectric barrier. It may also be that approximations in the model are compensated for by the diffusion coefficients. For example, in the Nernst-Planck equation **Error! Reference source not found.**, it is the product $D_i\rho_i$ that appears, and therefore an incorrect density may be compensated for by an effective diffusion coefficient. This is certainly a possibility. However, charge neutrality gives a good upper bound on ρ_i. The protein charge density is large in RyR (13 M for Asp-4899) and diffusion is limited in a only 15 Å-long segment of the pore. In that case, the measured 800 pS conductance for K^+ can only be achieved in a one-dimensional PNP theory with a diffusion coefficient around 4% of bulk (see Appendix). By this estimate, any error compensation there is seems to be limited to a factor significantly less than 10, or a Boltzmann factor of less than 2 kT. Certainly, they are the *effective* diffusion coefficients needed in such a model.

References (Supplementary Material)

1. Gillespie, D., L. Xu, Y. Wang, and G. Meissner. 2005. (De)constructing the ryanodine receptor: Modeling ion permeation and selectivity of the calcium release channel. J. Phys. Chem. B 109:15598-15610.

2. Xu, L., Y. Wang, D. Gillespie, and G. Meissner. 2006. Two rings of negative charges in the cytosolic vestibule of type-1 ryanodine receptor modulate ion fluxes. Biophys. J. 90:443-453.

3. Gao, L., D. Balshaw, L. Xu, A. Tripathy, C. Xin, and G. Meissner. 2000. Evidence for a Role of the Lumenal M3-M4 Loop in Skeletal Muscle Ca^{2+} Release Channel (Ryanodine Receptor) Activity and Conductance. Biophys. J. 79:828-840.

4. Wang, Y., L. Xu, D. A. Pasek, D. Gillespie, and G. Meissner. 2005. Probing the Role of Negatively Charged Amino Acid Residues in Ion Permeation of Skeletal Muscle Ryanodine Receptor. Biophys. J. 89:256-265.

5. Ludtke, S. J., I. I. Serysheva, S. L. Hamilton, and W. Chiu. 2005. The Pore Structure of the Closed RyR1 Channel. Structure 13:1203-1211.

6. Samsó, M., T. Wagenknecht, and P. D. Allen. 2005. Internal structure and visualization of transmembrane domains of the RyR1 calcium release channel by cryo-EM. Nature Structural & Molecular Biology 12:539-544.

7. Nonner, W. and B. Eisenberg. 1998. Ion Permeation and Glutamate Residues Linked by Poisson-Nernst-Planck Theory in L-Type Calcium Channels. Biophys. J. 75:1287-1305.

8. Nonner, W., L. Catacuzzeno, and B. Eisenberg. 2000. Binding and Selectivity in L-Type Calcium Channels: A Mean Spherical Approximation. Biophys. J. 79:1976-1992.

9. Boda, D., D. D. Busath, D. J. Henderson, and S. Sokolowski. 2000. Monte Carlo Simulations of the Mechanism of Channel Selectivity: The competition between Volume Exclusion and Charge Neutrality. J. Phys. Chem. B *104*:8903-8910.

10. Boda, D., M. Valiskó, B. Eisenberg, W. Nonner, D. J. Henderson, and D. Gillespie. 2006. The effect of protein dielectric coefficient on the ionic selectivity of a calcium channel. J. Chem. Phys. 125:034901.

11. Boda, D., M. Valiskó, B. Eisenberg, W. Nonner, D. J. Henderson, and D. Gillespie. 2007. Combined effect of pore radius and protein dielectric coefficient on the selectivity of a calcium channel. Phys. Rev. Lett. 98:168102.

12. Chen, D., L. Xu, A. Tripathy, G. Meissner, and B. Eisenberg. 1997. Permeation through the calcium release channel of cardiac muscle. Biophys. J. 73:1337-1354.

13. Chen, D. P., L. Xu, A. Tripathy, G. Meissner, and B. Eisenberg. 1999. Selectivity and Permeation in Calcium Release Channel of Cardiac Muscle: Alkali Metal Ions. Biophys. J. 76:1346-1366.

14. Chen, D., L. Xu, B. Eisenberg, and G. Meissner. 2003. Calcium ion permeation through the calcium release channel (ryanodine receptor) of cardiac muscle. J. Phys. Chem. B 107:9139-9145.

15. Chen, D., J. Lear, and B. Eisenberg. 1997. Permeation through an open channel: Poisson-Nernst-Planck theory of a synthetic ionic channel. Biophys. J. 72:97-116.

16. Miedema, H., A. Meter-Arkema, J. Wierenga, J. Tang, B. Eisenberg, W. Nonner, H. Hektor, D. Gillespie, and W. Meijberg. 2004. Permeation Properties of an Engineered Bacterial OmpF Porin Containing the EEEE-Locus of Ca^{2+} Channels. Biophys. J. 87:3137-3147.

17. Miedema, H., M. Vrouenraets, J. Wierenga, D. Gillespie, B. Eisenberg, W. Meijberg, and W. Nonner. 2006. Ca^{2+} Selectivity of a Chemically Modified OmpF with Reduced Pore Volume. Biophys. J. 91:4392-4400.

18. Rodriguez-Contreras, A., W. Nonner, and E. N. Yamoah. 2002. Ca^{2+} transport properties and determinants of anomalous mole fraction effects of single voltage-gated Ca^{2+} channels in hair cells from bullfrog saccule. J Physiol 538:729-745.

19. Hollerbach, U., D. P. Chen, D. D. Busath, and B. Eisenberg. 2000. Predicting Function from Structure Using the Poisson-Nernst-Planck Equations: Sodium Current in the Gramicidin A Channel. Langmuir 16:5509-5514.

20. Cardenas, A. E., R. D. Coalson, and M. G. Kurnikova. 2000. Three-Dimensional Poisson-Nernst-Planck Theory Studies: Influence of Membrane Electrostatics on Gramicidin A Channel Conductance. Biophys. J. 79:80-93.

21. Furini, S., F. Zerbetto, and S. Cavalcanti. 2006. Application of the Poisson-Nernst-Planck Theory with Space-Dependent Diffusion Coefficients to KcsA. Biophys. J. 91:3162-3169.

22. Mamonov, A. B., M. G. Kurnikova, and R. D. Coalson. 2006. Diffusion constant of K+ inside Gramicidin A: A comparative study of four computational methods. Biophys. Chem. 124:268-278.

23. Bostick, D. and M. L. Berkowitz. 2003. The Implementation of Slab Geometry for Membrane-Channel Molecular Dynamics Simulations. Biophys. J. 85:97-107.

24. Laudernet, Y., T. Cartailler, P. Turq, and M. Ferrario. 2003. A microscopic description of concentrated potassium fluoride aqueous solutions by molecular dynamics simulation. J. Phys. Chem. B 107:2354-2361.

25. Allen, T. W., S. Kuyucak, and S.-H. Chung. 2000. Molecular dynamics estimates of ion diffusion in model hydrophobic and KcsA potassium channels. Biophys. Chem. 86:1-14.

26. Lindsay, A. R., S. D. Manning, and A. J. Williams. 1991. Monovalent cation conductance in the ryanodine receptor-channel of sheep cardiac muscle sarcoplasmic reticulum. J. Physiol. (London) 439:463-480.

27. Fawcett, W. R. 1999. Thermodynamic Parameters for the Solvation of Monatomic Ions in Water. J. Phys. Chem. B 103:11181-11185.

28. Gouaux, E. and R. MacKinnon. 2005. Principles of Selective Ion Transport in Channels and Pumps. Science 310:1461-1465.

29. Smith, G. R. and M. S. P. Sansom. 1998. Dynamic Properties of Na^+ Ions in Models of Ion Channels: A Molecular Dynamics Study. Biophys. J. 75:2767-2782.

30. Corry, B., T. W. Allen, S. Kuyucak, and S.-H. Chung. 2001. Mechanisms of Permeation and Selectivity in Calcium Channels. Biophys. J. 80:195-214.

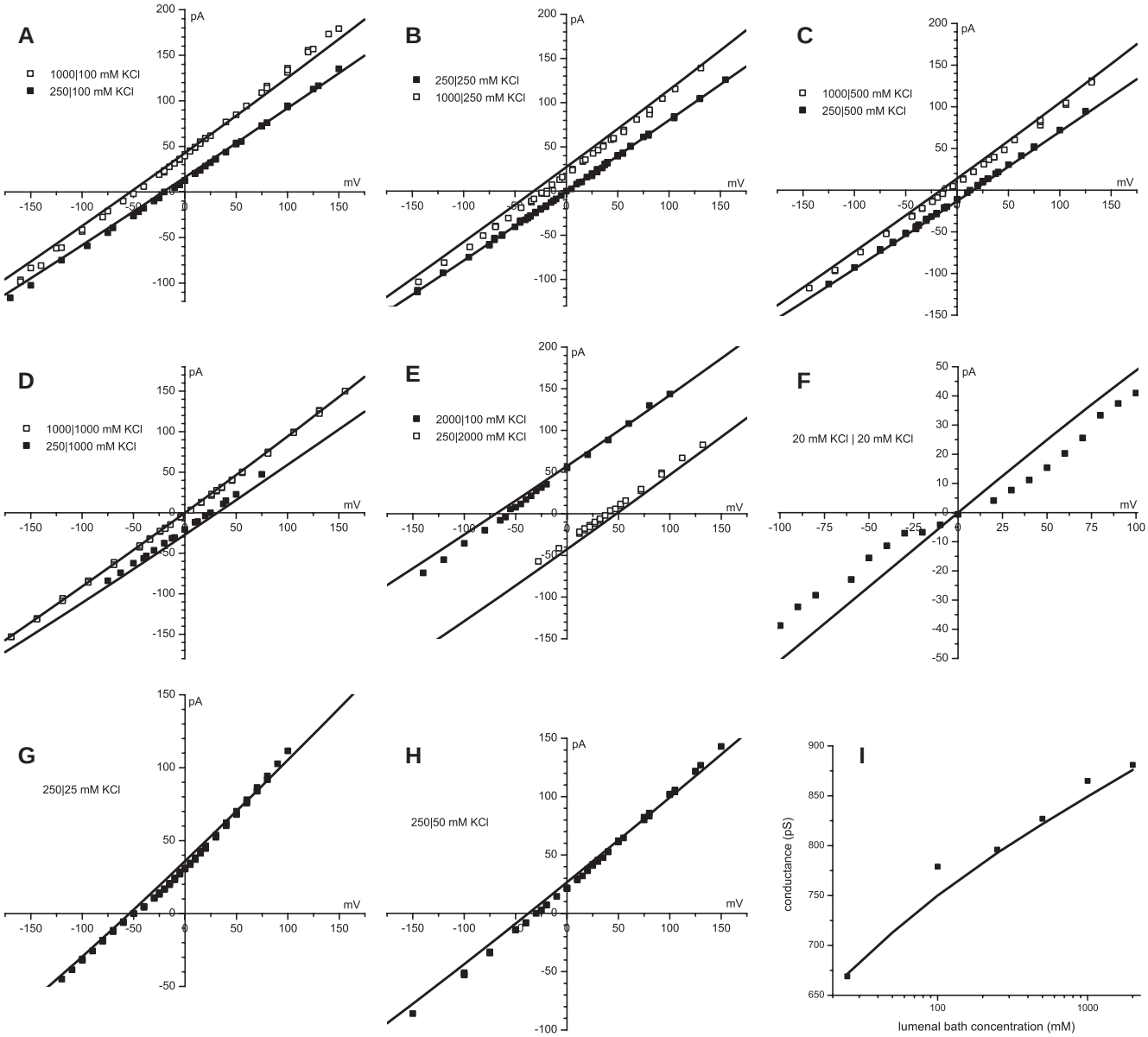

Figure S1. (A-H) Current/voltage curves in KCl. (I) The conductance at reversal potential with cytosolic [K^+] held at 250 mM and lumenal [K^+] is varied. For both experiment and theory the current/voltage curve was fitted with a line and the slope is plotted. In this and the following figures, concentrations are listed as cytosolic | lumenal. The solid lines are the model and symbols are the experimental data. Comparing panel I and Fig. 16B of Supplementary Material Ref. 1 summarizes the improvements due to the new RyR model; in general the computed current/voltage curves are more linear and the conductances are significantly closer to experimental values, especially in cases where the lumenal concentration is low. With the exception of panel F, this experimental data was previously published by Chen et al. (12). The data in panel F was previously published by Gillespie et al. (1).

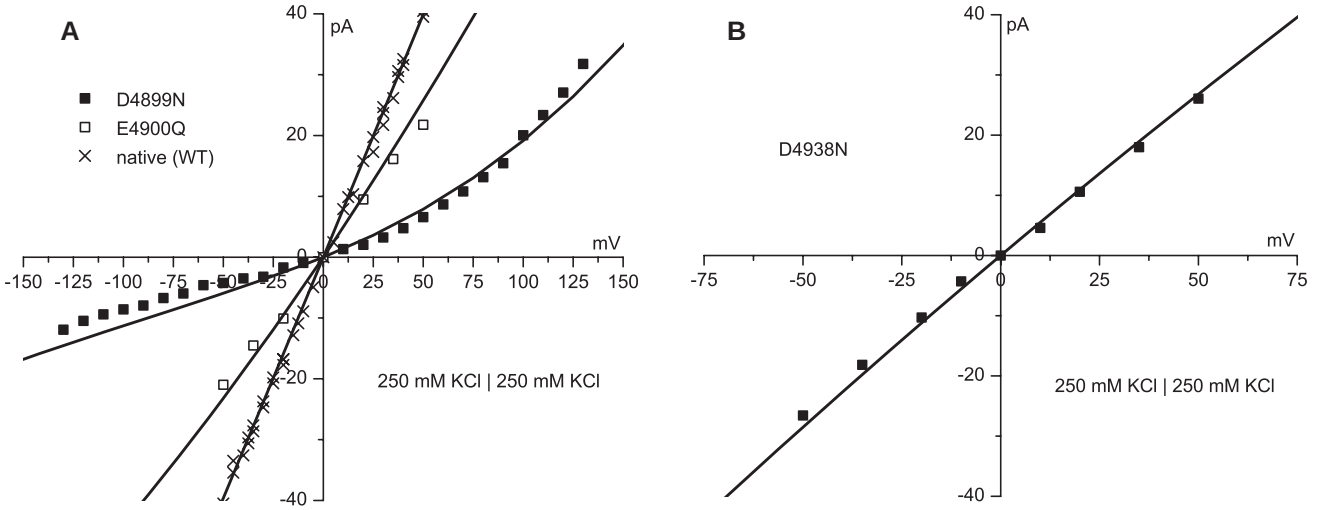

Figure S2. Current/voltage curves of (A) native (WT) RyR (×) and the mutants D4899N (■) and E4900Q (□) and (B) the D4938N mutant in 250 mM symmetric KCl. The D4899N data was previously published by Gao et al. (3), E4900Q by Wang et al. (4), and D4938N by Xu et al. (2).

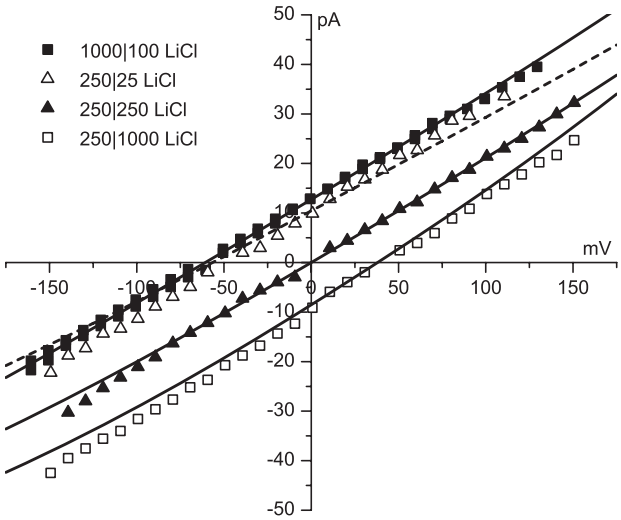

Figure S3. Current/voltage curves in LiCl. The dashed line is the model result for 250 mM cytosolic and 25 mM lumenal bath concentrations (Δ). Compared to the previous model, the dashed line reproduces the data much better. This experimental data was previously published by Chen et al. (13).

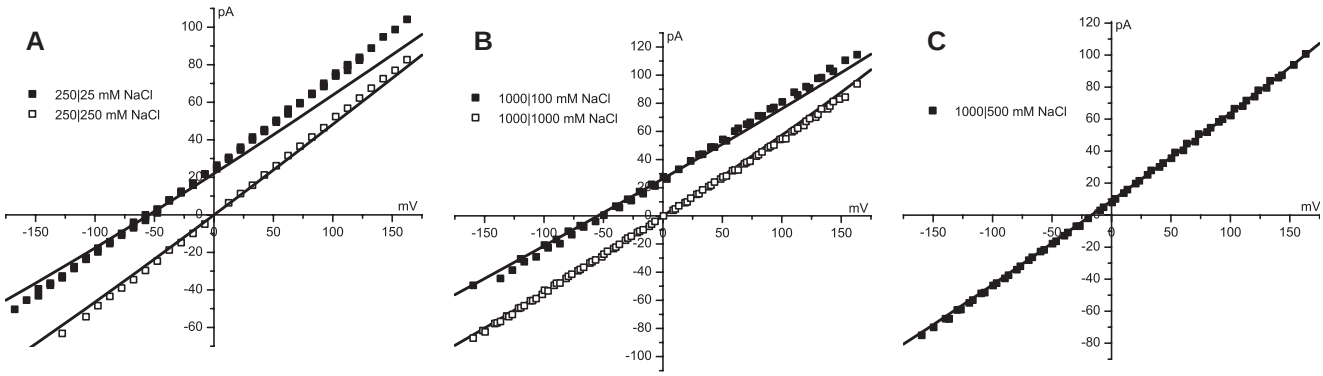

Figure S4. Current/voltage curves in NaCl. Compared to the previous model, the current/voltage curves are more linear and reproduce the data better in very asymmetric solutions. This experimental data was previously published by Chen et al. (13).

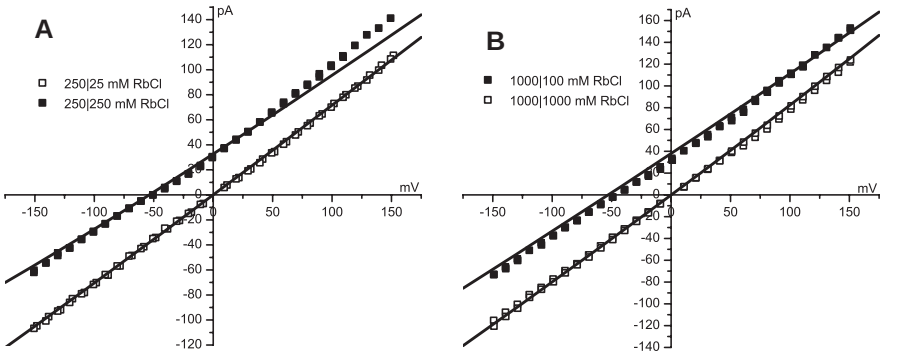

Figure S5. Current/voltage curves in RbCl. Compared to the previous model, the current/voltage curves are more linear and reproduce the data better in very asymmetric solutions. This experimental data was previously published by Chen et al. (13).

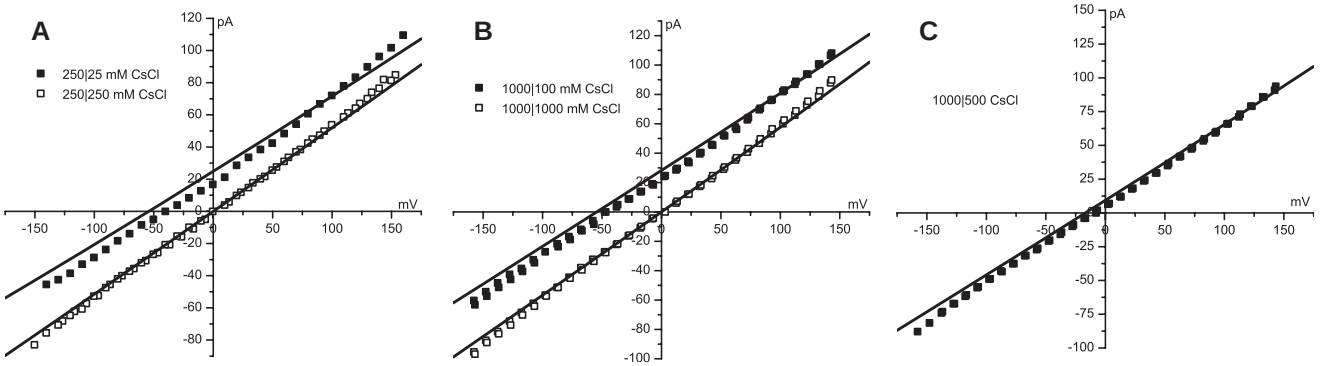

Figure S6. Current/voltage curves in CsCl. Compared to the previous model, the current/voltage curves are more linear and reproduce the data better in very asymmetric solutions. This experimental data was previously published by Chen et al. (13).

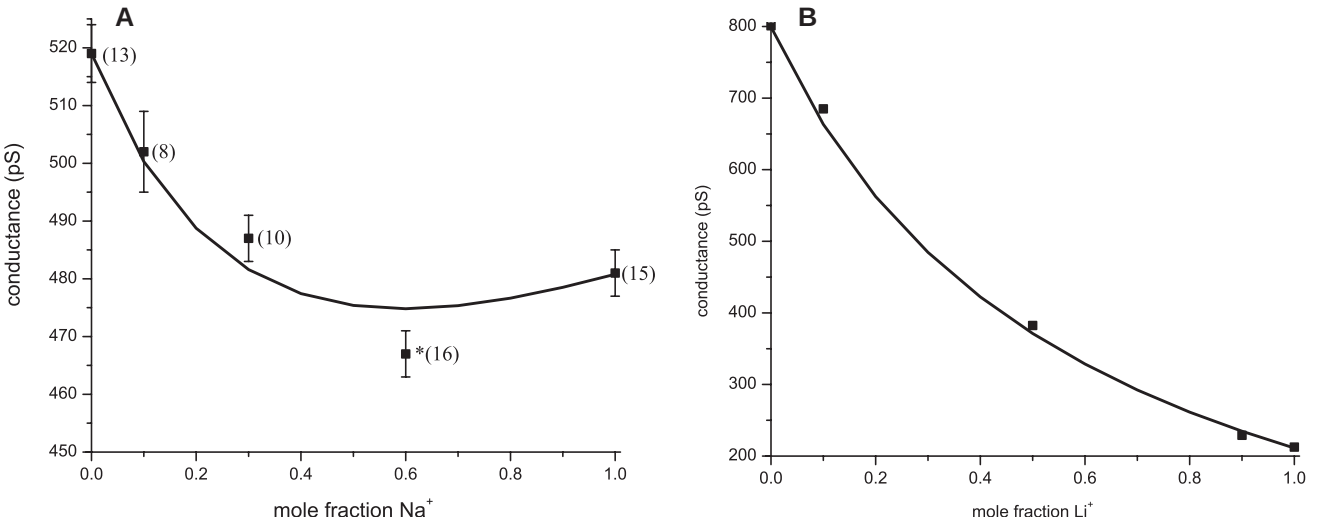

Figure S7. Mole fraction experiments at 250 mM total cation concentration in symmetric solutions. (A) NaCl and CsCl mixtures. The experimental point at mole fraction 0.6 is statistically significantly different than the point at mole fraction 1 ($p < 0.05$). The number of experiments is shown in parentheses. This experimental data was previously published by Gillespie et al. (1), but this is the first publication of this data with the multiple experiments. (B) LiCl and KCl mixtures. This experimental data at these concentrations was previously published by Chen et al. (13). This mole fraction experiment was first performed at 210 mM total cation concentration by Lindsay et al. (26).

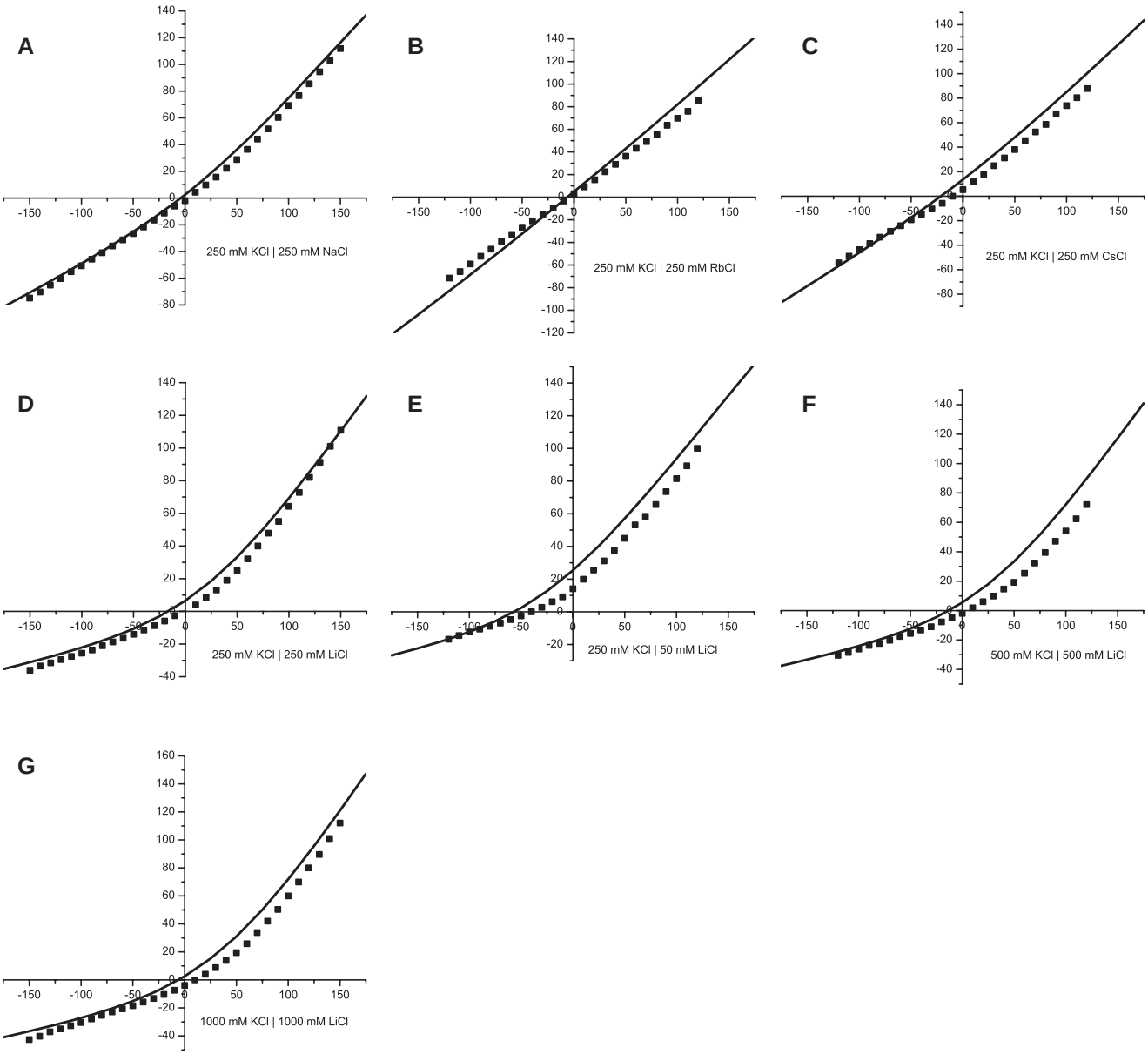

Figure S8. Current/voltage curves in bi-ionic conditions. This experimental data was previously published by Chen et al. (13).

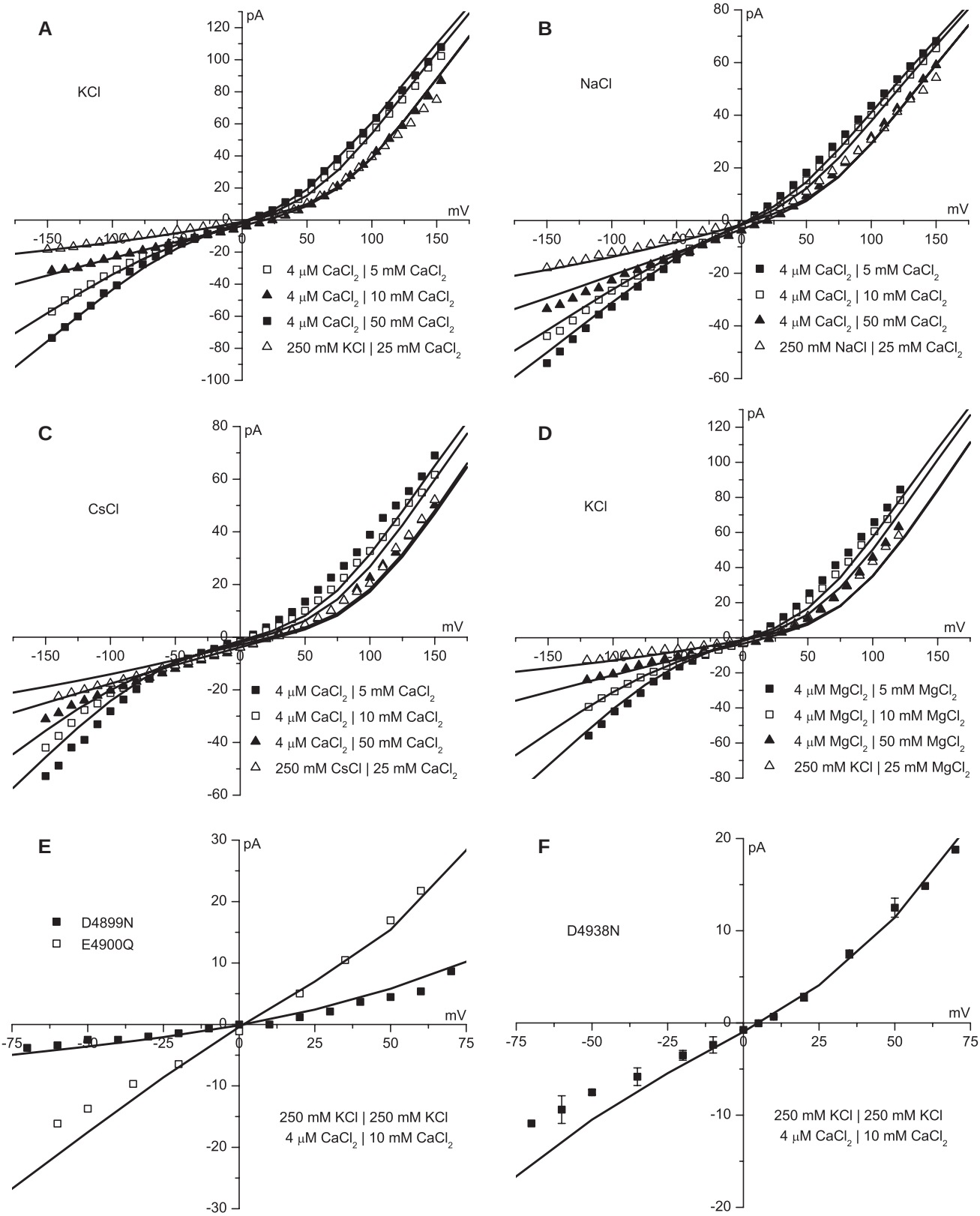

Figure S9. Current/voltage curves with divalent and monovalent cations. (A) KCl and $CaCl_2$. (B) NaCl and $CaCl_2$. (C) CsCl and $CaCl_2$. (D) KCl and $MgCl_2$. In both baths are 250 mM monovant-Cl and in the lumenal bath is 5 mM (■), 10 mM (□), and 50 mM (▲) divalent-Cl_2; or the cytosolic bath contains 250 mM cytosolic monovant-Cl while the lumenal bath contains 25 mM lumenal divalent-Cl_2 (Δ). Current/voltage curves of (E) the D4899N (■) and E4900Q (□) mutants and (F) the D4938N mutant in 250 mM symmetric KCl and 10 mM lumenal $CaCl_2$. Compared to the previous model, the current/voltage curves of Cs^+/Ca^{2+} mixtures and Na^+/Ca^{2+} mixture reproduce the data better. The data in panels A–D were first published by Chen et al. (14). The D4899N data (panel E) was previously published by Gao et al. (3), E4900Q (panel E) by Wang et al. (4), and D4938N (panel F) by Xu et al. (2).